Original Article

Correlation between magnetic resonance imaging (MRI) features and lesion size in focal nodular hyperplasia of the liver

Yijun Pan[1,2], Wei Liu[3], Yan Shan[1,2], Jiang Lin[1,2], Pengju Xu[1,2]

[1]Department of Radiology, Zhongshan Hospital, Fudan University, Shanghai, China; [2]Shanghai Institute of Medical Imaging, Shanghai, China; [3]Department of Nuclear Medicine, Fudan University Shanghai Cancer Center, Shanghai, China

Contributions: (I) Conception and design: Y Pan, P Xu; (II) Administrative support: J Lin, P Xu; (III) Provision of study materials or patients: P Xu; (IV) Collection and assembly of data: Y Pan, W Liu, Y Shan; (V) Data analysis and interpretation: Y Pan, Y Shan; (VI) Manuscript writing: All authors; (VII) Final approval of manuscript: All authors.

Correspondence to: Pengju Xu, MD. Department of Radiology, Zhongshan Hospital, Fudan University, No. 180 Fenglin Road, Xuhui District, Shanghai 200032, China; Shanghai Institute of Medical Imaging, Shanghai, China. Email: xpjbfc@163.com.

Background: Focal nodular hyperplasia (FNH) in the liver is a benign lesion and the relationship between lesion size and imaging features is yet to be established. We aimed to develop and validate a scoring system to assess the relationship between magnetic resonance imaging (MRI) features and lesion size in FNH.

Methods: This cross-sectional study was conducted at Zhongshan Hospital, Fudan University in Shanghai, China, from August 2019 and March 2023. Three hundred and seven patients with 363 surgically confirmed FNHs were retrospectively enrolled (training set: 254 lesions, validation set: 109 lesions). Lesions were divided into large (>3 cm) and small (≤3 cm) groups according to the diameter. Multivariate logistic regression was used to assess imaging features associated with lesion size in the training set. A scoring system was constructed and verified. The discrimination and calibration performance of the scoring system were evaluated by the receiver operating characteristic and calibration curve.

Results: In the training set, a round appearance (P<0.001) and hyperintense on arterial, portal and delayed phase (P=0.004) were more frequently observed in small FNHs, whereas a lobulated appearance [odds ratio (OR) =4.155, 95% confidence interval (CI): 2.023–8.536; P<0.001], feeding artery (OR =7.083, 95% CI: 2.970–16.892; P<0.001), radiating septa (OR =3.747, 95% CI: 1.682–8.347; P=0.001), central scar (OR =2.838, 95% CI: 1.284–6.273; P=0.010), hyperintense on arterial phase, hyper to isointense on portal phase, and isointense on delayed phase (OR =3.539, 95% CI: 1.650–7.595; P=0.001) were significantly associated with large FNHs. A scoring system derived from these variables showed an area under the curve of 0.888 (95% CI: 0.843–0.924) and 0.896 (95% CI: 0.821–0.945) in training and validation set respectively.

Conclusions: Through scoring MRI features, it can be observed that these features contribute differently to the diagnosis of FNH depending on its size.

Keywords: Focal nodular hyperplasia (FNH); liver neoplasms; magnetic resonance imaging (MRI)

Submitted Apr 24, 2024. Accepted for publication Sep 20, 2024. Published online Nov 13, 2024.
doi: 10.21037/qims-24-836
View this article at: https://dx.doi.org/10.21037/qims-24-836

Introduction

Focal nodular hyperplasia (FNH) in the liver is the second most common benign liver lesion after hepatic haemangiomas (1). It is regarded as a regenerative nodule of mature hepatocytes surrounding a central fibrotic scar with vascular malformation and ductular reaction (2). An accurate and confident diagnosis of FNH is of clinical relevance, as

surgery and invasive procedures are not recommended for asymptomatic patients.

The use of hepatobiliary contrast agents, especially gadoxetic acid (Gd-EOB-DTPA), has improved the diagnostic performance of liver magnetic resonance imaging (MRI) for FNH (3,4). However, the available studies are heterogeneous with limited samples and at high risk for bias, suggesting an overestimation of diagnostic accuracy for Gd-EOB-DTPA-enhanced MRI (5). Furthermore, the overlapping features for FNH and hepatocellular adenoma on hepatobiliary phase images indicate a lower specificity of Gd-EOB-DTPA-enhanced magnetic resonance (MR) than previously reported (6,7). Currently, gadoxetic acid-enhanced MR is recommended as a second diagnostic step after the focal liver lesion is detected on routine liver MR (8), but it requires two MR scans in a short period of time, which increases the financial burden on patients.

Routine liver MRI and contrast-enhanced ultrasound (CEUS) are the first-line imaging modalities for the diagnosis of FNH, with a specificity close to 100% when central scar, feeding artery with radiating branches and typical enhancement pattern are all evident (8-11). However, distinctive characteristics may not always be easily identified in FNHs of various size. Studies have shown that the typical imaging features of FNH, such as the spoke-wheel pattern and central scar, are strongly associated with the lesion size and are more frequently noted in FNHs >3 cm (12,13). On the contrary, Wang *et al.* (14) studied 85 FNHs by using CEUS and reported that the spoke-wheel pattern and feeding artery were not size-dependent in FNHs. These findings are not fully documented in MRI studies owing to the ambiguous definition of the signs.

Recently, a scoring system based on a regression model has emerged as an intuitive and effective tool for differential diagnosis and prognostic prediction (15,16). The scoring system allows a simple risk stratification by assigning points to statistically significant variables. Although studies have identified typical imaging features for FNH, a formalized scoring system associated with lesion size has not been developed.

Therefore, our study aimed to develop and validate a scoring system to assess the relationship between MRI features and lesion size in FNH. We present this article in accordance with the STROBE reporting checklist (available at https://qims.amegroups.com/article/view/10.21037/qims-24-836/rc).

Methods

This study was conducted in accordance with the Declaration of Helsinki (as revised in 2013). The study was reviewed and approved by the Institutional Review Board of Zhongshan Hospital, Fudan University (B2022-437), and the requirement for written informed consent was waived due to the retrospective nature of the study.

Study population

We retrospectively identified 369 patients with surgically confirmed FNH in our institution between August 2019 and March 2023. The inclusion criteria were as follows: (I) age ≥18 years; (II) patients without cirrhosis or hepatitis; (III) patients without a history of hepatic malignancies; (IV) patients who underwent preoperative MRI within 1 month before surgery. Patients were excluded for the following reasons: (I) with cirrhosis or chronic hepatitis (n=38); (II) previous history of hepatocellular carcinoma (HCC), liver metastasis, or other hepatic malignancies (n=18); (III) absence of dynamic enhanced MRI before surgery (n=6). The final study population included 307 patients with 363 FNHs. For the analysis, the 363 FNHs were divided into training (n=254) and validation (n=109) set in a 7:3 ratio based on the surgical timing. The flowchart of patient enrolment was presented in *Figure 1*. A total of 147 patients (47.9%) patients met surgical indication due to abdominal pain or symptomatic organ compression. Additionally, 79 patients (25.7%) with a history of other cancers or atypical imaging features were recommended for surgical resection, and the remaining patients chose surgical treatment mainly due to an increase of lesion size during follow-up. The treatment decision was made based on surgeon's discretion and patients' wishes.

Conventional MRI acquisition

MRI examinations were performed by using 3.0-T scanners (Siemens Healthcare, Prisma and UIHMR770). Routine liver protocols included spoiled gradient-echo T1-weighted in-phase and opposed-phase imaging, turbo spin-echo T2-weighted imaging (T2WI), diffusion-weighted imaging (DWI, b values =0, 50, and 500 s/mm^2) and dynamic contrast-enhanced (DCE) imaging. The apparent diffusion coefficient (ADC) was automatically calculated by the MR units and presented as an ADC map. The gadopentetate dimeglumine (Gd-DTPA) was administered intravenously

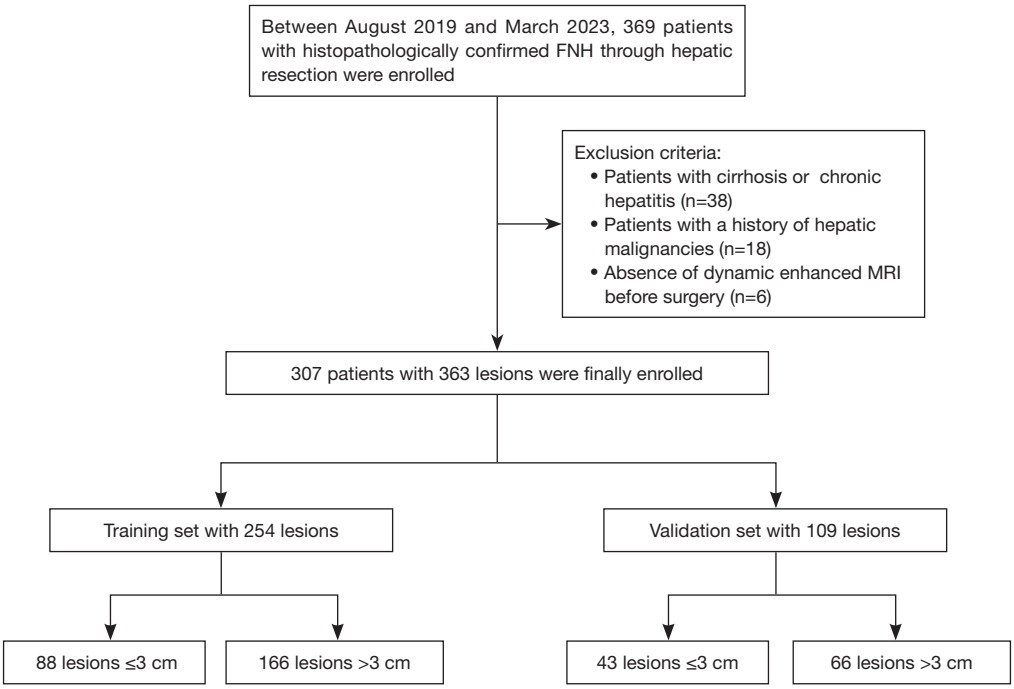

Figure 1 Flowchart of study population. FNH, focal nodular hyperplasia; MRI, magnetic resonance imaging.

at a rate of 2 mL/s and a dose of 0.1 mmol/kg, followed by a 20-mL saline flush. The arterial, portal, and delayed phase images were obtained respectively at 20–30, 70–90, and 160–180 s.

Imaging analysis

All MR images were reviewed independently by two abdominal radiologists (Y.P. and Y.S., with 5 and 20 years of experience, respectively) who were informed of the pathologic results. A third experienced abdominal radiologist (P.X. with 28 years of experience) was invited to resolve disagreements between the two observers.

MR features were evaluated as follows: (I) lesion number (single or multiple), (II) lesion location (right, left or caudate lobe), (III) lesion size, defined as the maximum diameter on transverse images, was measured on arterial phase images, and all lesions are categorized as large (>3 cm) or small (≤3 cm) based on the maximum diameter (12-14,17), (IV) morphology (round or lobulated), (V) the presence of hepatic steatosis and intralesional fat, defined as a signal dropout on T1-weighted opposed-phase images compared to in-phase images, (VI) relative signal intensity of the lesion compared to the surrounding liver parenchyma (hyperintense, isointense or hypointense) on T1-weighted imaging (T1WI), T2WI and DWI images, (VII) lesion homogeneity on T2WI except the scar (homogenous or heterogeneous), (VIII) enhancing capsule, defined as smooth uniform enhancing border assessed in portal or delayed phase, (IX) central scar, defined as a central or eccentric area showed hyperintense on T2WI or delayed phase, (X) feeding artery, defined as hypertrophic artery directed towards the lesion and larger than the branches at the same depth during the arterial phase, (XI) radiating septa, defined as radiating enhancement from the center of the lesion with low-signal fibrous bands, (XII) enhancement patterns are defined as three types: hyperintense on arterial, portal and delayed phase; hyperintense on arterial phase, hyper to isointense on portal phase, and isointense on delayed phase; hyperintense on arterial phase and hypointense on portal and delayed phase, (XIII) for ADC value analysis, region of interest (ROI) was drawn on the diffusion-weighted images with b=500 mm^2/s to include the largest areas of FNH, and then copied the ROIs to the ADC map to measure ADC values. Large vessels and artifacts were excluded. The measurements were performed two times and the ADC values were averaged for analysis. The Gd-EOB-DTPA-enhanced MR protocol and analysis were shown in supplementary material Appendix 1.

Statistical analysis

All analyses were performed by using SPSS (version 20.0, Chicago IL, USA) and R Software (version 4.2.2). Continuous variables were presented as mean ± standard deviation and were compared with Student's *t*-test. The age of patients was presented as median (interquartile range, IQR) (non-Gaussian distribution). Categorical variables were presented as numbers (percentages) and were compared with the Chi-squared test or Fisher's exact test. Univariate logistic regression was performed in the training set, and the significant variables with P<0.1 were further included in the multivariate logistic analysis via stepwise selection. The regression coefficients were regarded as the weights for the variables in the score model. In this study, the presence of a central scar was defined as a score of 1. The scores for the other variables were obtained by dividing their regression coefficients by that of the central scar. The scoring system was evaluated by a receiver operating characteristic (ROC) curve and verified in the validation set. The calibration performance was evaluated with a calibration curve. Interobserver agreement of MRI features was evaluated by calculating the Cohen κ coefficient (0.8–1, excellent; 0.6–0.79, good; 0.4–0.59, moderate; 0.2–0.39, fair; 0–0.19, poor). The differences between the results of the Gd-EOB-DTPA-enhanced MRI and scoring system based on conventional MRI was compared by a paired Chi-squared test. The level of statistical significance was set at 2-sided P<0.05.

Results

Patients and lesion characteristics

Based on the selection criteria, 307 patients who underwent liver resection and conventional MR examination were finally enrolled in this study. Most patients were young (median: 31 years; IQR: 26–39 years) and women (59.2%). Thirty patients exhibited multiple lesions, twenty-five patients had two FNHs, four had three, and one had four. The most common location of the lesion was the right lobe (54.0%), followed by the left lobe (38.3%) and caudate lobe (7.7%). As the size and location of the targeted lesion varied across all cases, any potential for confusion between them was effectively eliminated. A total of 363 FNHs were divided into the training set (n=254; 166 for size >3 cm, 88 for size ≤3 cm) and validation set (n=109; 66 for size >3 cm, 43 for size ≤3 cm).

MRI features for FNHs with different sizes

The MRI features of FNHs in training and validation set are presented in *Table 1* and Table S1. In the training set, the presence of hepatic steatosis, intralesional fat and the ADC values were not significantly different between large and small FNHs. The lobulated appearance (75.9% *vs.* 26.1%, P<0.001) and heterogeneous intensity on T2WI (31.9% *vs.* 6.8%, P<0.001) were more common in large lesions. Compared to small lesions, the large one exhibited a higher frequency of isointense on T1WI (54.2% *vs.* 39.8%, P=0.028) and T2WI (48.2% *vs.* 34.1%, P=0.031), whereas signals on DWI showed no significant difference in two groups. The presence of the enhancing capsule (39.8% *vs.* 8.0%, P<0.001), central scar (84.3% *vs.* 38.6%, P<0.001), feeding artery (56.0% *vs.* 10.2%, P<0.001) and radiating septa (77.1% *vs.* 31.8%, P<0.001) were more frequently noted in large lesions. For dynamic enhancement pattern, all FNHs were hyperintense against the surrounding liver parenchyma on arterial phase. More than half of lesions showed hyper to isointense on portal phase and isointense on delayed phase (68.1% in large FNHs, 53.4% in small FNHs). Others showed hyperintense (28.3% in large FNHs, 46.6% in small FNHs) or hypointense (3.6% in large FNHs, 0% in small FNHs) appearance on both portal and delayed phase. The difference of enhancement pattern between two groups were statistically significant (P=0.004) (*Figures 2*,*3*).

The κ value of the interobserver agreement for lesion size was 0.905. The interobserver agreement for MRI features ranged from 0.635 to 0.883, corresponding to a good to excellent agreement between observers (Table S2).

Univariate and multivariate analyses

In the training set, univariate analysis showed that several MRI features exhibited a significant association with large FNH, including a lobulated appearance [odds ratio (OR) =8.902; 95% confidence interval (CI): 4.916–16.121; P<0.001], heterogeneous intensity on T2WI (OR =6.410; 95% CI: 2.630–15.622; P<0.001), isointense on T1WI (OR =1.793; 95% CI: 1.060–3.031; P=0.028) and T2WI (OR =1.798; 95% CI: 1.0526–3.072; P=0.030), the presence of enhancing capsule (OR =7.637; 95% CI: 3.322–17.556; P<0.001), central scar (OR =8.552; 95% CI: 4.696–15.574; P<0.001), feeding artery (OR =11.182; 95% CI: 5.258–23.782; P<0.001), radiating septa (OR =7.218; 95%

Table 1 MR features of FNHs in training and validation set

Variable	Training cohort			Validation cohort		
	≤3 cm (n=88)	>3 cm (n=166)	P value	≤3 cm (n=43)	>3 cm (n=66)	P value
Size (cm)	2.0±0.7	5.5±2.0	<0.001	2.1±0.6	5.5±2.0	<0.001
Hepatic steatosis	25 (28.4)	47 (28.3)	0.987	15 (34.9)	17 (25.8)	0.307
Intralesional fat	6 (6.8)	7 (4.2)	0.552	4 (9.3)	1 (1.5)	0.078
Morphology			<0.001			<0.001
Round	65 (73.9)	40 (24.1)		34 (79.1)	16 (24.2)	
Lobulated	23 (26.1)	126 (75.9)		9 (20.9)	50 (75.8)	
DWI			0.860			0.598
Isointense	10 (11.4)	16 (9.6)		6 (14.0)	7 (10.6)	
Hyperintense	78 (88.6)	150 (90.4)		37 (86.0)	59 (89.4)	
ADC ($\times10^{-3}$ mm^2/s)	1.6±0.4	1.7±0.4	0.661	1.7±0.4	1.7±0.5	0.702
T1WI			0.028			0.031
Hypointense	53 (60.2)	76 (45.8)		28 (65.1)	29 (43.9)	
Isointense	35 (39.8)	90 (54.2)		15 (34.9)	37 (56.1)	
T2WI			0.031			0.002
Isointense	30 (34.1)	80 (48.2)		9 (20.9)	33 (50.0)	
Hyperintense	58 (65.9)	86 (51.8)		34 (79.1)	33 (50.0)	
Homogeneity on T2WI			<0.001			0.191
Homogenous	82 (93.2)	113 (68.1)		37 (86.0)	50 (75.8)	
Heterogeneous	6 (6.8)	53 (31.9)		6 (14.0)	16 (24.2)	
Enhancing capsule	7 (8.0)	66 (39.8)	<0.001	2 (4.7)	27 (40.9)	0.001
Central scar	34 (38.6)	140 (84.3)	<0.001	16 (37.2)	56 (84.8)	<0.001
Feeding artery	9 (10.2)	93 (56.0)	<0.001	8 (18.6)	29 (43.9)	0.006
Radiating septa	28 (31.8)	128 (77.1)	<0.001	11 (25.6)	50 (75.8)	<0.001
Enhancement pattern			0.004			0.003
Hyper/hyper/hyper	41 (46.6)	47 (28.3)		26 (60.5)	20 (30.3)	
Hyper/hyper-iso/iso	47 (53.4)	113 (68.1)		17 (39.5)	45 (68.2)	
Hyper/hypo/hypo	0 (0)	6 (3.6)		0 (0)	1 (1.5)	

Data are presented as mean ± standard deviation or number (%). MR, magnetic resonance; FNH, focal nodular hyperplasia; DWI, diffusion-weighted imaging; ADC, apparent diffusion coefficient; T1WI, T1-weighted imaging; T2WI, T2-weighted imaging; hyper, hyperintense; iso, isointense; hypo, hypointense.

CI: 4.055–12.846; P<0.001) and hyper/hyper to iso/iso-enhancement pattern (OR =2.097; 95% CI: 1.222–3.598; P=0.007) (*Table 2*). A multivariate logistic regression model was subsequently fitted to those variables, and the following MRI features remained statistical significance: lobulated appearance (OR =4.155; 95% CI: 2.023–8.536; P<0.001), the presence of feeding artery (OR =7.083; 95% CI: 2.970–16.892; P<0.001), radiating septa (OR =3.747; 95% CI: 1.682–8.347; P=0.001), central scar (OR =2.838; 95% CI: 1.284–6.273; P=0.010), and hyper/hyper to iso/iso-enhancement pattern (OR =3.539; 95% CI: 1.650–7.595; P=0.001) (*Table 2*).

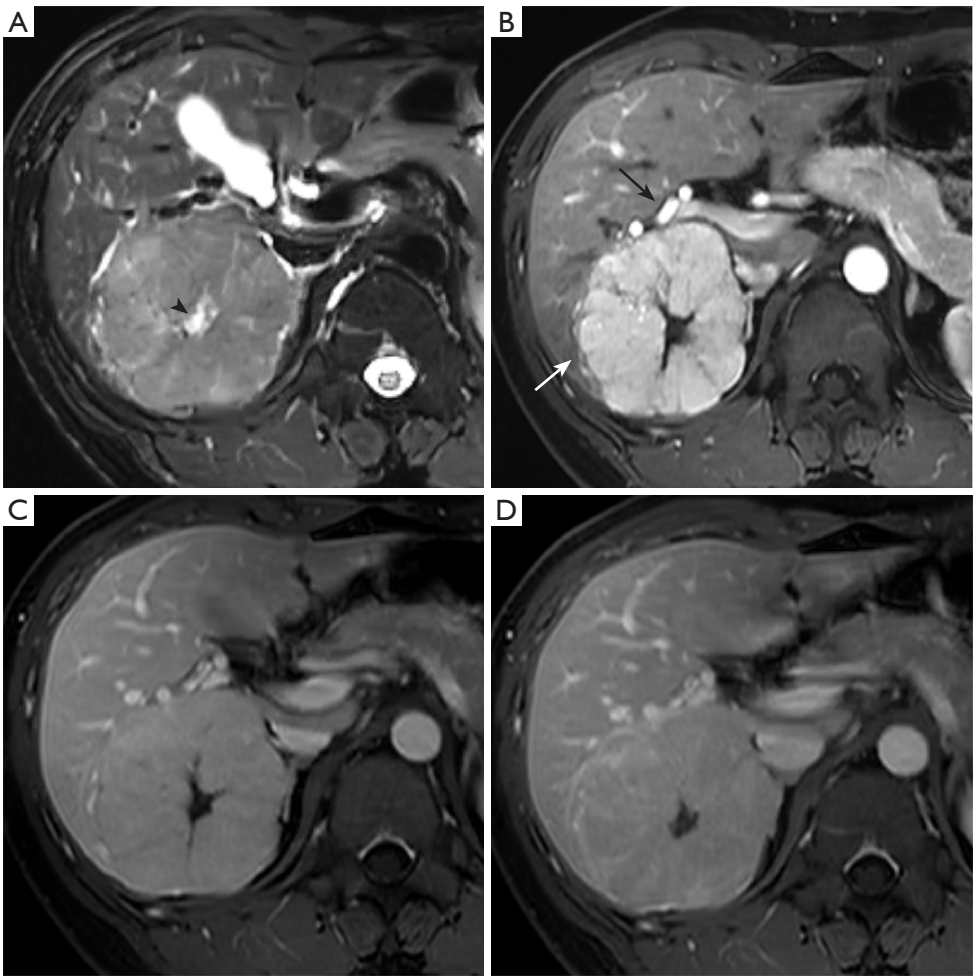

Figure 2 T2-weighted image (A) shows a lobulated and large FNH (8.4 cm) with central scar (black arrowhead). Arterial phase image (B) shows radiating septa (white arrow) and enlarged hepatic artery (black arrow). It shows isointense on portal (C) and delayed (D) phases. FNH, focal nodular hyperplasia.

Development and validation of score system

A simple scoring system based on regression coefficients was developed to evaluate the significance of different MRI features in diagnosing large FNH. We modified the multivariate model into a scoring system with points: lobulated appearance (1.5 points), feeding artery (2 points), radiating septa (1.5 points), central scar (1 point), and hyper/hyper to iso/iso-enhancement pattern (1 point) (*Table 3*). The scoring system showed good discrimination performance in the training and validation set, as reflected by the area under the curve (AUC) of 0.888 (95% CI: 0.843–0.924, cutoff >2.5 points) (*Figure 4A*) and 0.896 (95% CI: 0.821–0.945) (*Figure 4B*), respectively. Moreover, the scoring system also showed good calibration in the training (*Figure 5A*) and validation (*Figure 5B*) set. In addition, 7 FNHs appear atypically washout on MRI. However, the scores ranged from 3 to 6 for these lesions according to our scoring system, indicating a high probability of a large FNH (*Figure 6*).

To determine the usefulness of the scoring system, we compared the results obtained separately by using Gd-EOB-DTPA-enhanced MRI and scoring system based on conventional MRI. In the entire cohort, 31 patients (16 male and 15 female) with a mean age of 30 years underwent Gd-EOB-DTPA-enhanced MRI (large FNHs, n=18; small FNHs, n=14) (Figure S1). In the hepatobiliary phase (HBP), peripheral ring-like with hypointense central core was more frequently observed in small FNHs

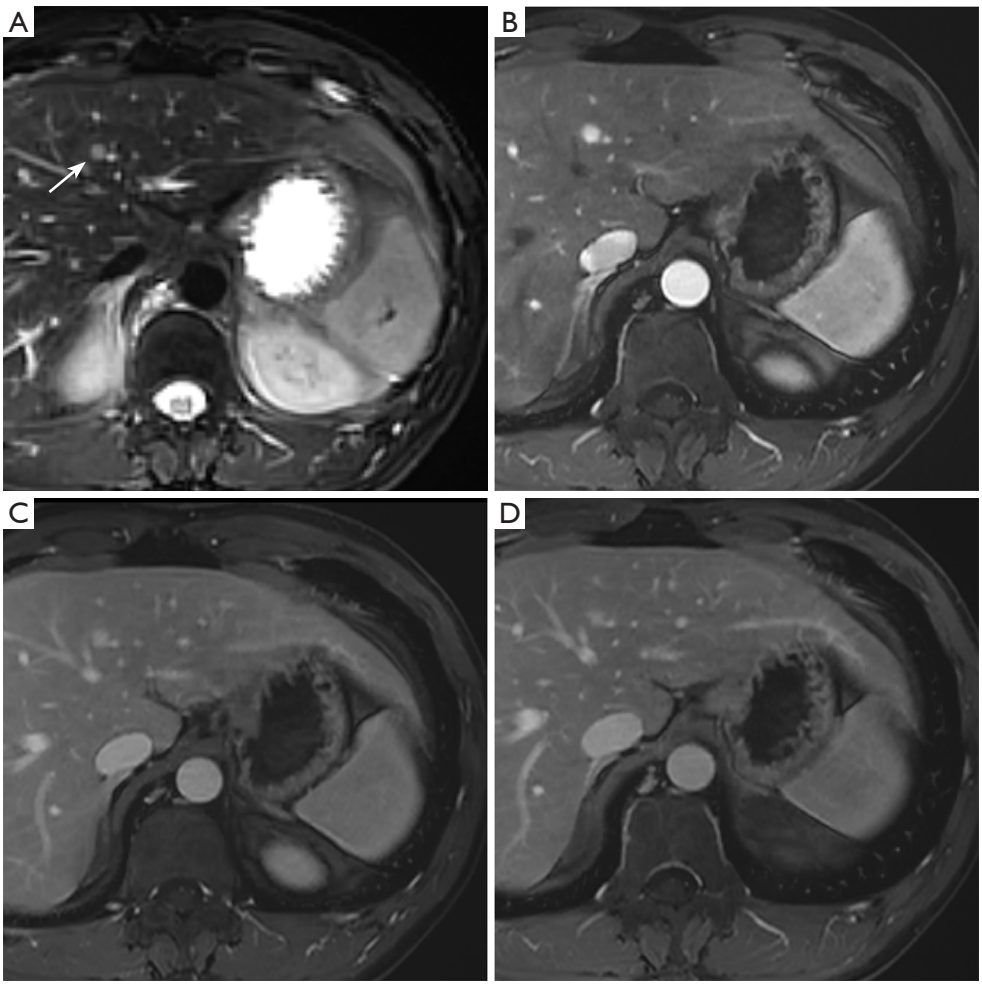

Figure 3 T2-weighted image (A) shows a round and small FNH (0.8 cm, white arrow). The lesion shows marked enhancement on arterial phase (B) and hyperintense on portal (C) and delayed (D) phases. Central scar, feeding artery or radiating septa was absent. FNH, focal nodular hyperplasia.

(50%, 7/14), whereas homogeneous hyperintense was more common in large FNHs (50%, 9/18) (Table S3). No significant difference was observed between these two methods in the detection of small (P=0.070) and large FNHs (P=0.500) (Table S4).

Discussion

In this study, we found a round appearance and hyper/hyper/hyper-enhancement pattern were more common in small FNHs. The lobulated appearance, presence of feeding artery, radiating septa, central scar, and hyper/hyper to iso/iso-enhancement pattern were strongly associated with large FNHs. The weight of these MRI features is presented as a score in the final model to facilitate clinical practice.

FNH is usually a benign liver lesion and does not require specific treatment or follow-up, which requires a well-designed algorithm to efficiently identify it in clinical practice. Our experience suggests that most FNHs are easily recognized on MR images when the size of the lesion is taken into account. Although the association between imaging features and lesion size has been explored (12-14,17), previous studies are limited by the small sample size of FNH or lack of comparison with the histological diagnosis. To better determine the relationship between suggestive signs and lesion size, we present the largest series of FNHs from a retrospective cohort of patients who underwent surgical liver resection.

Table 2 Univariate and multivariate analysis of MR feature in training set

Variable	Univariate analysis			Multivariate analysis			
	OR	95% CI	P value	OR	95% CI	P value	Regression coefficient
Hepatic steatosis	0.995	0.561–1.765	0.987	–	–	–	–
Intralesional fat	0.602	0.196–1.849	0.375	–	–	–	–
Morphology	8.902	4.916–16.121	<0.001	4.155	2.023–8.536	<0.001	1.425
DWI	1.201	0.520–2.773	0.668	–	–	–	–
ADC	1.160	0.598–2.248	0.658	–	–	–	–
T1WI	1.793	1.060–3.031	0.028	–	–	–	–
T2WI	1.798	1.0526–3.072	0.030	–	–	–	–
Heterogeneous	6.410	2.630–15.622	<0.001	–	–	–	–
Enhancing capsule	7.637	3.322–17.556	<0.001	–	–	–	–
Central scar	8.552	4.696–15.574	<0.001	2.838	1.284–6.273	0.010	1.043
Feeding artery	11.182	5.258–23.782	<0.001	7.083	2.970–16.892	<0.001	1.958
Radiating septa	7.218	4.055–12.846	<0.001	3.747	1.682–8.347	0.001	1.321
Enhancement pattern							
Hyper/hyper/hyper	1			–	–	–	
Hyper/hyper-iso/iso	2.097	1.222–3.598	0.007	3.539	1.650–7.595	0.001	1.164
Hyper/hypo/hypo	–	–	0.999	–	–	–	

MR, magnetic resonance; OR, odds ratio; CI, confidence interval; DWI, diffusion-weighted imaging; ADC, apparent diffusion coefficient; T1WI, T1-weighted imaging; T2WI, T2-weighted imaging; hyper, hyperintense; iso, isointense; hypo, hypointense.

As for the feeding artery, a detection rate of 67.1% was reported by CEUS (14), while a computed tomography (CT) study yielded a lower rate of 33.9% (18). In our study, MRI demonstrated a similar detection rate of the feeding artery as CT of FNH (38.3%). CEUS identifies feeding arteries through continuous cine imaging, with a higher sensitivity than CT and MR. Apart from the lack of real-time images, another limitation of MR is a relatively low spatial resolution, which may lead to the overlooking of small arteries. In agreement with the findings reported by Brancatelli *et al*. (18), the feeding artery was more common in large FNHs, with a detection rate of 52.6% in FNHs >3 cm and 13.0% in FNHs ≤3 cm in our study. Notably, the presence of the feeding artery showed the highest weight in the scoring system for the characterization of large FNH. Histologically, FNH is thought to be a hyperplastic regenerative response to congenital vascular abnormalities or vascular damage (19). The imaging features correspond well to the histologic findings, the enlarged feeding arteries can be identified at the peripheral, septal, or central of the lesion during the arterial phase (18).

The spoke-wheel pattern has been recognized as a key finding for the confirmative diagnosis of FNH, with a detection rate ranging from 23.5% to 77.4% on CEUS (17,20,21). However, no reports have been found to describe this pattern in FNH on MRI, which is difficult to detect when the branches of the feeding artery are too small. In the present study, the determination of this pattern largely depends on the detection of radiating septa. In our large series, the radiating septa was detected on MRI in 217 out of 363 (59.8%) lesions, which is comparable to CEUS. Radiating septa was more frequently observed in FNHs larger than 3 cm and was a significant factor in the final scoring model. However, Bertin *et al.* (17) and Wang *et al.* (14) reported that the spoke-wheel pattern was more common in small FNHs. They took centrifugal filling into account, and this ambiguous definition may lead to misinterpretation of the images.

Another typical feature is the central scar, which occurs in more than half of FNH lesions (22). This sign is evident

Table 3 MR imaging score system for FNH lesions >3 cm

Variable	Score
Morphology	
Round	0
Lobulated	1.5
Central scar	
Absence	0
Presence	1
Feeding artery	
Absence	0
Presence	2
Radiating septa	
Absence	0
Presence	1.5
Enhancement pattern	
Hyper/hyper/hyper	0
Hyper/hyper-iso/iso	1
Hyper/hypo/hypo	0

MR, magnetic resonance; FNH, focal nodular hyperplasia; hyper, hyperintense; iso, isointense; hypo, hypointense.

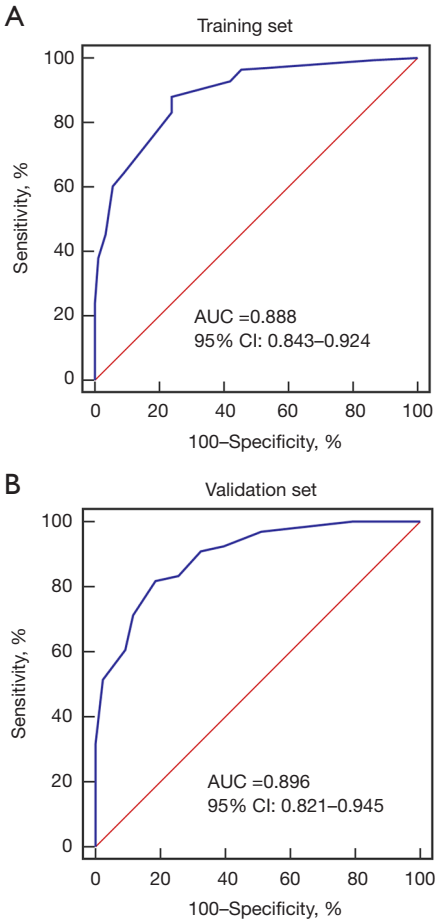

Figure 4 ROC of the scoring system in the training set (A) and validation set (B). AUC, area under the curve; CI, confidence interval; ROC, receiver operating curves.

in most FNHs larger than 3 cm but rarely observed in those less than 3 cm (12,14,23). In our study, the central scar was detected in 84.5% of the large FNHs and 38.2% of the small FNHs. Although the central scar was a well-recognized indicator for FNH, it showed the lowest odds ratio in the multivariate analysis. One potential explanation is that scar is a histological alteration secondary to the occlusion or fibrosis of central artery (24). Liu *et al.* (25) reported that vascular endothelial cells in FNH contribute to the fibrotic process by expressing sclerostin, which may eventually promote the formation of the fibrous scar. In addition, the presence of a scar is not specific to FNH, large hemangioma, beta-catenin adenomas, and fibrolamellar HCC could also exhibit this feature (26,27).

The enhancement pattern of FNH also appears to be related to the lesion size. The predominance of marked enhancement during arterial phase without washout is consistent with the previous reports (28,29). In this study, large FNHs tended to exhibit isointense during the delayed phase, whereas small lesions showed hyper-enhancement. The degree of fibrosis in lesions may be a contributing factor. Although 1.9% (7/363) of FNHs appeared atypically washout, which is slightly lower than in previous studies (3,26), a more accurate diagnosis can still be made by combining the weights of other MRI features. We recommend this new scoring system for clinical practice, as it allows a quick and comprehensive assessment for FNH, even with a few atypical signs. The diagnostic accuracy for the scoring system was comparable to that of Gd-EOB-DTPA-enhanced MRI. This improvement could help to optimize clinical workflow, avoid unnecessary imaging and reduce patient's cost.

There are several limitations in this study. Firstly, this is a retrospective study without external validation. However, it is the largest set of FNHs ever studied, and all lesions were surgically resected and underwent histological analysis. Secondly, there may be confirmation bias regarding the

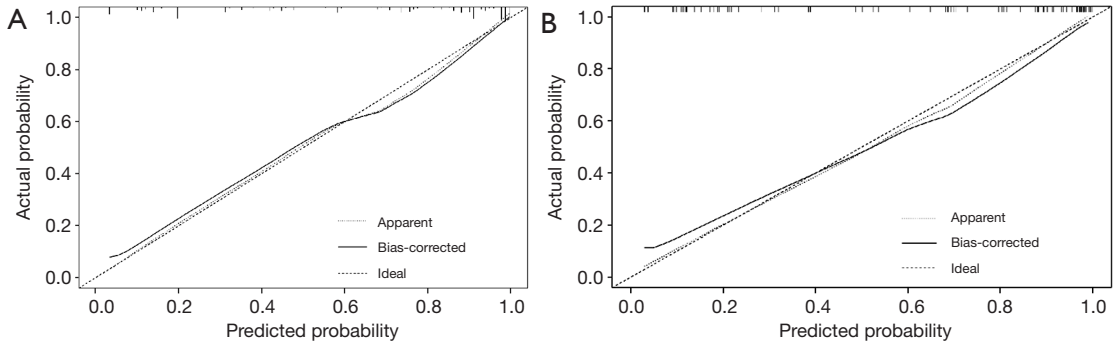

Figure 5 The calibration curve of the scoring system in the training (A) and validation (B) sets.

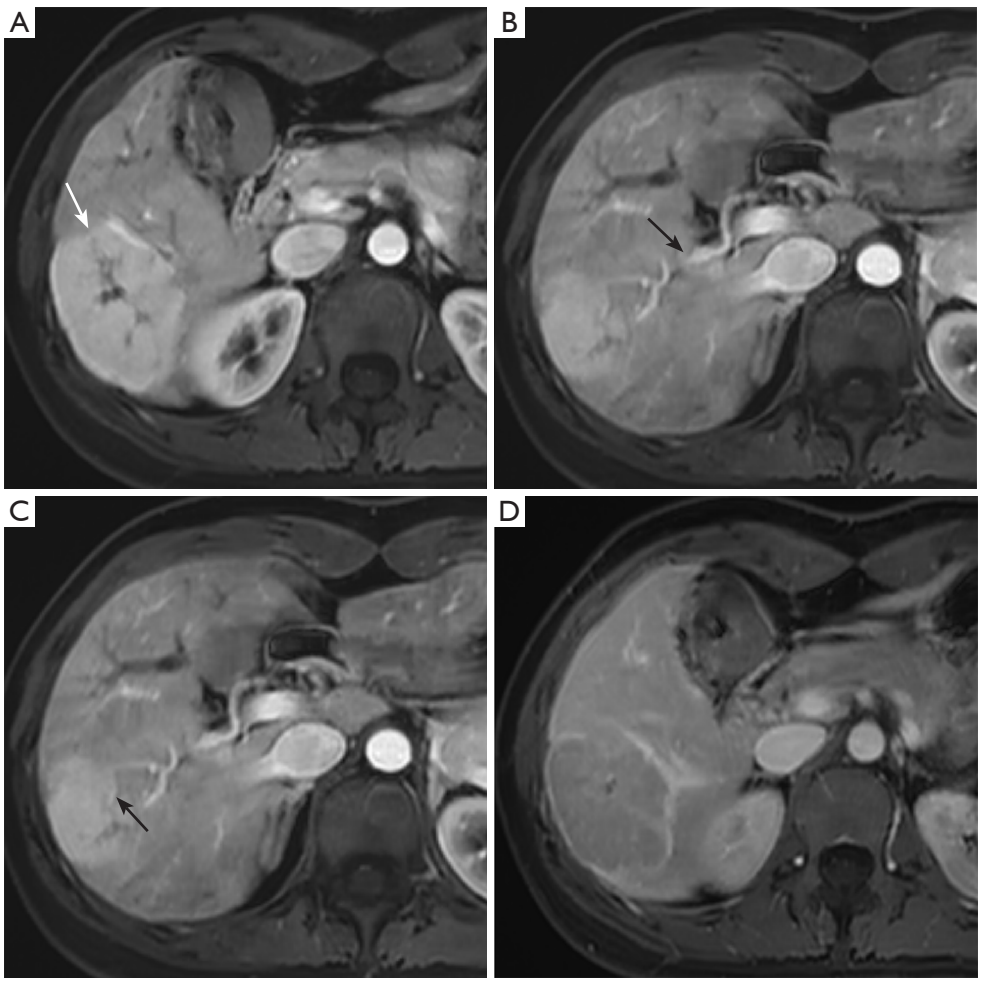

Figure 6 Arterial phase image shows a lobulated large FNH (5.8 cm) with radiating septa [white arrow (A)] and enlarged hepatic artery [black arrows (B,C)]. It has a washout appearance on delayed phase image (D), which obtained a score of 5. FNH, focal nodular hyperplasia.

detection of imaging features when observers were informed that all lesions were FNH. The 95% CIs for ORs of several features were too wide in the univariate and multivariate analyses. This may be due to the relatively small number of lesions within a certain category of risk factors (i.e., enhancing capsule and feeding artery were observed in only 7 and 9 small lesions, respectively). Thirdly, only a small subset of the cohort underwent Gd-EOB-DTPA-enhanced MRI, thus the sample size was reduced for these analyses. Finally, other liver tumors were not included because the aim of the study was to focus on the characterization of FNH. The clinical usefulness of this score system in differentiating FNH from other liver tumors needs to be further investigated. But for the patients with clinical suspicion of FNH or a few atypical MRI features, the scores of imaging features may improve diagnostic accuracy. A prospective, multicenter study including a variety of liver lesions is needed to validate the scoring system in the future.

Conclusions

In conclusion, the scoring system gives different weights to MRI features according to the correlation of each feature with lesion size. It can be observed that these MRI features contribute differently to the diagnosis of FNH depending on its size.

Acknowledgments

Funding: This study was supported by Science and Technology Commission of Shanghai Municipality (Shanghai 2022 "Science and Technology Innovation Action Plan" Medical Innovation Research Special Project) (No. 22Y11910900 to P.X.), and Shanghai Municipal Health Commission (Shanghai Municipal Key Clinical Specialty) (No. shslczdzk03202 to P.X.).

Footnote

Reporting Checklist: The authors have completed the STROBE reporting checklist. Available at https://qims.amegroups.com/article/view/10.21037/qims-24-836/rc

Conflicts of Interest: All authors have completed the ICMJE uniform disclosure form (available at https://qims.amegroups.com/article/view/10.21037/qims-24-836/coif). The authors have no conflicts of interest to declare.

Ethical Statement: The authors are accountable for all aspects of the work in ensuring that questions related to the accuracy or integrity of any part of the work are appropriately investigated and resolved. This study was conducted in accordance with the Declaration of Helsinki (as revised in 2013). The study was reviewed and approved by the Institutional Review Board of Zhongshan Hospital, Fudan University (B2022-437), and the requirement for written informed consent was waived due to the retrospective nature of the study.

References

1. Kaltenbach TE, Engler P, Kratzer W, Oeztuerk S, Seufferlein T, Haenle MM, Graeter T. Prevalence of benign focal liver lesions: ultrasound investigation of 45,319 hospital patients. Abdom Radiol (NY) 2016;41:25-32.
2. Shanbhogue AK, Prasad SR, Takahashi N, Vikram R, Sahani DV. Recent advances in cytogenetics and molecular biology of adult hepatocellular tumors: implications for imaging and management. Radiology 2011;258:673-93.
3. Grazioli L, Bondioni MP, Haradome H, Motosugi U, Tinti R, Frittoli B, Gambarini S, Donato F, Colagrande S. Hepatocellular adenoma and focal nodular hyperplasia: value of gadoxetic acid-enhanced MR imaging in differential diagnosis. Radiology 2012;262:520-9.
4. Bilreiro C, Soler JC, Ayuso JR, Caseiro-Alves F, Ayuso C. Diagnostic value of morphological enhancement patterns in the hepatobiliary phase of gadoxetic acid-enhanced MRI to distinguish focal nodular hyperplasia from hepatocellular adenoma. Radiol Med 2021;126:1379-87.
5. McInnes MD, Hibbert RM, Inácio JR, Schieda N. Focal Nodular Hyperplasia and Hepatocellular Adenoma: Accuracy of Gadoxetic Acid-enhanced MR Imaging--A Systematic Review. Radiology 2015;277:413-23.
6. Grieser C, Steffen IG, Kramme IB, Bläker H, Kilic E, Perez Fernandez CM, Seehofer D, Schott E,

Hamm B, Denecke T. Gadoxetic acid enhanced MRI for differentiation of FNH and HCA: a single centre experience. Eur Radiol 2014;24:1339-48.
7. Denecke T, Steffen IG, Agarwal S, Seehofer D, Kröncke T, Hänninen EL, Kramme IB, Neuhaus P, Saini S, Hamm B, Grieser C. Appearance of hepatocellular adenomas on gadoxetic acid-enhanced MRI. Eur Radiol 2012;22:1769-75.
8. EASL Clinical Practice Guidelines on the management of benign liver tumours. J Hepatol 2016;65:386-98.
9. Ronot M, Vilgrain V. Imaging of benign hepatocellular lesions: current concepts and recent updates. Clin Res Hepatol Gastroenterol 2014;38:681-8.
10. Grazioli L, Morana G, Kirchin MA, Schneider G. Accurate differentiation of focal nodular hyperplasia from hepatic adenoma at gadobenate dimeglumine-enhanced MR imaging: prospective study. Radiology 2005;236:166-77.
11. Khanna M, Ramanathan S, Fasih N, Schieda N, Virmani V, McInnes MD. Current updates on the molecular genetics and magnetic resonance imaging of focal nodular hyperplasia and hepatocellular adenoma. Insights Imaging 2015;6:347-62.
12. Ungermann L, Eliás P, Zizka J, Ryska P, Klzo L. Focal nodular hyperplasia: spoke-wheel arterial pattern and other signs on dynamic contrast-enhanced ultrasonography. Eur J Radiol 2007;63:290-4.
13. Bartolotta TV, Taibbi A, Matranga D, Malizia G, Lagalla R, Midiri M. Hepatic focal nodular hyperplasia: contrast-enhanced ultrasound findings with emphasis on lesion size, depth and liver echogenicity. Eur Radiol 2010;20:2248-56.
14. Wang W, Chen LD, Lu MD, Liu GJ, Shen SL, Xu ZF, Xie XY, Wang Y, Zhou LY. Contrast-enhanced ultrasound features of histologically proven focal nodular hyperplasia: diagnostic performance compared with contrast-enhanced CT. Eur Radiol 2013;23:2546-54.
15. Wang S, Tian S, Li Y, Zhan N, Guo Y, Liu Y, Xu J, Ma Y, Zhang S, Song S, Geng W, Xia H, Ma P, Wang X, Liao T, Duan Y, Jin Y, Dong W. Development and validation of a novel scoring system developed from a nomogram to identify malignant pleural effusion. EBioMedicine 2020;58:102924.
16. Rhee H, Choi SH, Park JH, Cho ES, Yeom SK, Park S, Han K, Lee SS, Park MS. Preoperative magnetic resonance imaging-based prognostic model for mass-forming intrahepatic cholangiocarcinoma. Liver Int 2022;42:930-41.
17. Bertin C, Egels S, Wagner M, Huynh-Charlier I, Vilgrain V, Lucidarme O. Contrast-enhanced ultrasound of focal nodular hyperplasia: a matter of size. Eur Radiol 2014;24:2561-71.
18. Brancatelli G, Federle MP, Grazioli L, Blachar A, Peterson MS, Thaete L. Focal nodular hyperplasia: CT findings with emphasis on multiphasic helical CT in 78 patients. Radiology 2001;219:61-8.
19. Nguyen BN, Fléjou JF, Terris B, Belghiti J, Degott C. Focal nodular hyperplasia of the liver: a comprehensive pathologic study of 305 lesions and recognition of new histologic forms. Am J Surg Pathol 1999;23:1441-54.
20. Dioguardi Burgio M, Ronot M, Salvaggio G, Vilgrain V, Brancatelli G. Imaging of Hepatic Focal Nodular Hyperplasia: Pictorial Review and Diagnostic Strategy. Semin Ultrasound CT MR 2016;37:511-24.
21. Lee J, Jeong WK, Lim HK, Kim AY. Focal Nodular Hyperplasia of the Liver: Contrast-Enhanced Ultrasonographic Features With Sonazoid. J Ultrasound Med 2018;37:1473-80.
22. Kang TW, Jeong WK, Kim YY, Min JH, Kim YK, Kim SH, Sinn DH, Kim K. Comparison of Super-Resolution US and Contrast Material-enhanced US in Detection of the Spoke Wheel Sign in Patients with Focal Nodular Hyperplasia. Radiology 2021;298:82-90.
23. Kamel IR, Liapi E, Fishman EK. Focal nodular hyperplasia: lesion evaluation using 16-MDCT and 3D CT angiography. AJR Am J Roentgenol 2006;186:1587-96.
24. Wanless IR, Mawdsley C, Adams R. On the pathogenesis of focal nodular hyperplasia of the liver. Hepatology 1985;5:1194-200.
25. Liu Y, Zhang J, Wang Z, Ma J, Wang K, Rao D, Zhang M, Lin Y, Wu Y, Yang Z, Dong L, Ding Z, Zhang X, Fan J, Shi Y, Gao Q. Multi-omics characterization reveals the pathogenesis of liver focal nodular hyperplasia. iScience 2022;25:104921.
26. Zhang HT, Gao XY, Xu QS, Chen YT, Song YP, Yao ZW. Evaluation of the characteristics of hepatic focal nodular hyperplasia: correlation between dynamic contrast-enhanced multislice computed tomography and pathological findings. Onco Targets Ther 2016;9:5217-24.
27. Ganeshan D, Szklaruk J, Kundra V, Kaseb A, Rashid A, Elsayes KM. Imaging features of fibrolamellar hepatocellular carcinoma. AJR Am J Roentgenol 2014;202:544-52.
28. Morana G, Grazioli L, Kirchin MA, Bondioni MP, Faccioli N, Guarise A, Schneider G. Solid hypervascular liver lesions: accurate identification of true benign lesions on enhanced dynamic and hepatobiliary phase magnetic

resonance imaging after gadobenate dimeglumine administration. Invest Radiol 2011;46:225-39.
29. Minami Y, Nishida N, Kudo M. Imaging Diagnosis of Various Hepatocellular Carcinoma Subtypes and Its Hypervascular Mimics: Differential Diagnosis Based on Conventional Interpretation and Artificial Intelligence. Liver Cancer 2023;12:103-15.

Cite this article as: Pan Y, Liu W, Shan Y, Lin J, Xu P. Correlation between magnetic resonance imaging (MRI) features and lesion size in focal nodular hyperplasia of the liver. Quant Imaging Med Surg 2024;14(12):8758-8770. doi: 10.21037/qims-24-836